A Modified ETM Shaper For Double Pendulum Crane Control With Payload Hoisting

Trong Hieu Do*, Minh Duc Nguyen, and Minh Duc Duong

Hanoi University of Science and Technology

*Corresponding author. E-mail: hieu.dotrong@hust.edu.vn

Received: May 22, 2024; Accepted: Sep. 16, 2024

Overhead cranes are widely utilized in various industries and for transporting goods. However, the vibrations generated during operation can significantly impact the safety and efficiency of crane work. This issue becomes more critical when dealing with large-sized loads that cannot be overlooked. In such cases, the crane exhibits a double pendulum-like behaviour, and the load vibrations become multi-frequency. This paper proposes an Active Disturbance Rejection Control (ADRC) controller to control the crane's position combined with the Equal Shaping Time and Magnitude (ETM) input shaping technique to suppress load swinging during lifting operations. Simulations and experiments were performed to confirm the validity of the proposed method.

Keywords: Double-Pendulum Crane; ADRC; Input Shaping; Impulse Vector; Vibration Suppression

http://dx.doi.org/10.6180/jase.202508_28(8).0010

1. Introduction

The use of cranes is prevalent in many industries, including transportation, construction, and industry. One of the problems of cranes during operation is the vibration of the payload [1]. When the double pendulum effect occurs, the problem becomes more complex. In this situation, both the crane hook and the load vibrate in multi-frequency mode. In addition, changing the winch rope length and payload mass causes the vibration frequency to change, leading to anti-vibration control becoming extremely challenging.

To overcome the payload vibration and guarantee precise position control, feedback control strategies for double pendulum cranes have been proposed, such as tuned PID control [2], nonlinear quasi PID [3], nonlinear control [4], adaptive control [5, 6], optimal control [7, 8], sliding mode control [9–12], intelligent control [13–15], etc. For feedback controllers to take appropriate control actions, multiple sensors are required to measure the trolley position and the hook and payload oscillation angles. however, these additional sensors come at an extra cost, and accurately measuring the payload angles becomes challenging due to variations in payload masses, sizes, and shapes. The effects of the double-pendulum mechanism further compound this difficulty.

Feed-forward control, which is contrary to feedback control, has also been extensively employed for oscillation control in crane systems; for example, the two-mode input shaping has proven to be highly effective when implemented on double pendulum type cranes [16–18]. In addition, other feed-forward techniques such as command shaper [19–21], smoother [22–25] have been investigated. However, the majority of these studies have focused solely on scenarios involving constant vibration frequencies. In practical applications, cranes often need to transport loads while simultaneously lowering or lifting them to save time. This movement of the crane leads to changing rope length, resulting in variations in vibration frequencies. The vibration suppression control approaches for constant vibration frequencies may not be appropriate in the case of a variant vibration frequency. In Minh Duc et al. [26], a reference response-based vibration control technique is proposed for

a time-varying vibratory single pendulum crane system. However, the selected reference response and known time-varying vibration parameters are needed. In addition, the control technique is only for single-mode vibration.

To address the multi-mode time-varying frequency vibration issue that happens in double pendulum type cranes, this paper proposes Equal Shaping-Time and Magnitude (ETM) input shaping, in combination with Active Disturbance Rejection Control (ADRC) for control of the double pendulum type crane. At first, the ADRC is applied to control the trolley position precisely by using an Extended State Observer (ESO) to observe the disturbance and then reject it. After that, the ETM is designed to suppress the payload vibration. The robustness of the ETM approach allows for the suppression of the time-varying frequency vibrations, and choosing the appropriate frequencies for ETM designing is carefully evaluated. The effectiveness of the proposed control algorithm was validated through the implementation of simulations and experiments.

The remaining sections of the paper are organised as follows. section 2 introduces the mathematical model of the double pendulum crane. In section 3, the control system design is shown. The simulation result is described in section 4, and the experimental result is presented in section 5. Conclusion and further studies are described in section 6.

2. Double pendulum crane dynamical model

The model of the double pendulum crane is described in Fig. 1. x is the position of trolley, m is the trolley mass, m_1 is the hook mass, m_2 is the payload mass, l_1 is the cable length between trolley and hook, l_2 is the cable length between hook and payload, θ_1 is the 1^{st} sway angle, θ_2 is the 2^{nd} sway angle, the trolley is driven by the F_x and the payload is lifted by F_l. For simplicity, in this paper, the trolley, hook, and payload are considered as point masses. The friction force between the trolley and the rail is neglected. The dynamic model of the double pendulum crane is described by Lu et al. [5]:

$$\begin{gathered}(m+m_1+m_2)\,\ddot{x}+(m_1+m_2)\sin\theta_1\ddot{l}_1+\\ (m_1+m_2)\,l_1\cdot\ddot{\theta}_1\cos\theta_1+m_2l_2\ddot{\theta}_2\cos\theta_2\\ +2\,(m_1+m_2)\,\dot{\theta}_1\dot{l}_1\cos\theta_1-(m_1+m_2)\,l_1\dot{\theta}_1^2\sin\theta_1\\ -m_2l_2\dot{\theta}_2^2\sin\theta_2=F_x-D_t\dot{x}\end{gathered} \tag{1}$$

$$\begin{gathered}(m_1+m_2)\sin\theta_1\ddot{x}+(m_1+m_2)\,\ddot{l}_1+m_2l_2\sin(\theta_1-\theta_2)\,\ddot{\theta}_2\\ -(m_1+m_2)\,l_1\dot{\theta}_1^2-m_2l_2\cos(\theta_1-\theta_2)\,\dot{\theta}_2^2\\ -(m_1+m_2)\cdot g\cos\theta_1=F_l-D_l\dot{l}_1\end{gathered} \tag{2}$$

$$\begin{gathered}(m_1+m_2)\,l_1\cos\theta_1\ddot{x}+(m_1+m_2)\,l_1^2\ddot{\theta}_1\\ +m_2l_1l_2\cos(\theta_1-\theta_2)\cdot\ddot{\theta}_2+2\,(m_1+m_2)\,l_1\dot{\theta}_1\dot{l}_1\\ +m_2l_1l_2\sin(\theta_1-\theta_2)\,\dot{\theta}_2^2\\ +(m_1+m_2)\cdot gl_1\sin\theta_1=-D_1\dot{\theta}_1\end{gathered} \tag{3}$$

$$\begin{gathered}m_2l_2\cos\theta_2\ddot{x}+m_2l_2\sin(\theta_1-\theta_2)\,\ddot{l}_1\\ +m_2l_1l_2\cos(\theta_1-\theta_2)\cdot\ddot{\theta}_1+m_2l_2^2\ddot{\theta}_2\\ +2m_2l_2\cos(\theta_1-\theta_2)\,\dot{\theta}_1\dot{l}_1\\ -m_2l_1l_2\cdot\sin(\theta_1-\theta_2)\,\dot{\theta}_1^2+m_2gl_2\sin\theta_2=-D_2\dot{\theta}_2\end{gathered} \tag{4}$$

where g represents the gravity constant; D_t, D_l are viscous damping coefficients; D_1, D_2 are swing damping coefficients. The two linearised frequencies of the double pendulum are [27, 28]:

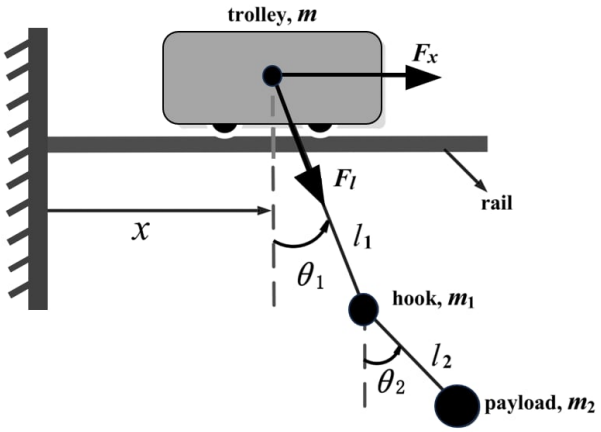

Fig. 1. The double pendulum crane system

$$\omega_{1,2}=\sqrt{\frac{g}{2}(\alpha\mp\sqrt{\beta})} \tag{5}$$

where:

$$\alpha=\frac{m_1+m_2}{m_1}\left(\frac{1}{l_1}+\frac{1}{l_2}\right) \tag{6}$$

$$\beta=\left(\frac{m_1+m_2}{m_1}\right)^2\left(\frac{1}{l_1}+\frac{1}{l_2}\right)^2-4\frac{m_1+m_2}{m_1}\frac{1}{l_1l_2} \tag{7}$$

The payload vibration of a double pendulum crane is the combination of two singlefrequency vibrations. To address this, this paper proposes the feedforward control approach as in Fig. 2 where double-mode ETM input shaping is considered for vibration suppression. Two ADRC controllers are applied to control trolley position and payload hoisting. The complete control scheme for the double pendulum crane is a combination of two ADRC controllers and double-mode input shaping.

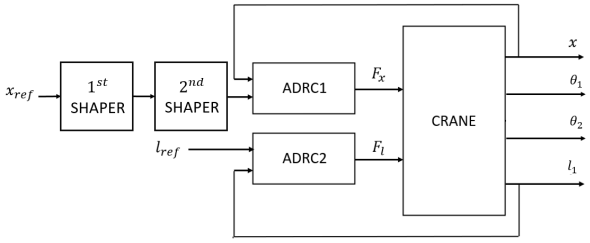

Fig. 2. Control system structure

3. Control system design

The overall proposed control structure can be depicted in Fig. 2, featuring two separate closed-loop control systems to regulate the position of the trolley and the cable length. ETM input shaping is used to suppress the vibration of the payload. As mentioned in the previous section, the dual swaying motions of the double-pendulum crane manifest as two distinct vibration frequencies. To effectively suppress these oscillations, we employ a twostage shaping strategy. Initially, a first shaper targets the suppression of the first frequency, followed by a second shaper designed to address the remaining vibration at the second frequency. The final control input is then generated by convolving these individual shapers.

3.1. ADRC concept

Active Disturbance Rejection Control, which was initially proposed in Han [29], is a control method to handle disturbances and uncertainties in a system. Because of its simplicity and effectiveness, ADRC is widely considered to replace PID controllers. First, Eqs. (1) and (2) are rewritten to the form as:

$$\ddot{x}(t) = f_x + b_{0x}F_x = f_x + \frac{1}{m + m_1 + m_2}F_x \tag{8}$$

$$\ddot{l}(t) = f_l + b_{0l}F_l = f_l + \frac{1}{m_1 + m_2}F_l \tag{9}$$

where

$f_x = -\left((m_1+m_2)\sin\theta_1\ddot{l}_1 + (m_1+m_2)\,l_1\cdot\ddot{\theta}_1\cos\theta_1 + m_2l_2\ddot{\theta}_2\cos\theta_2 + 2\,(m_1+m_2)\,\dot{\theta}_1\dot{l}_1\cos\theta_1 - (m_1+m_2)\,l_1\dot{\theta}_1^2\sin\theta_1 - m_2l_2\dot{\theta}_2^2\sin\theta_2 + D_t\dot{x}\right)/\,(m+m_1+m_2)$

$f_l = -\left((m_1+m_2)\sin\theta_1\ddot{x} + m_2l_2\sin(\theta_1-\theta_2)\,\ddot{\theta}_2 - (m_1+m_2)\,l_1\dot{\theta}_1^2 - m_2l_2\cos(\theta_1-\theta_2)\,\dot{\theta}_2{}^2 - (m_1+m_2)\cdot g\cos\theta_1 + D_l\dot{l}_1\right)/\,(m_1+m_2)$

In general, f_x and f_l contain nonlinearity and parameter uncertainties and can be considered as a total disturbance.

The Eqs. (8) and (9) have the general form of a second-order system as follows:

$$\ddot{y}(t) = f(t) + b_0u(t) \tag{10}$$

where $y(t)$ represents the output while $u(t)$ is the control signal and $f(t)$ is general disturbances. The control constant is denoted as b_0.

As a main point of ADRC, an Extended State Observer (ESO) is constructed to estimate the value of f, thereby compensating for the effect of f on the model. The extended observer is designed in the form of:

$$\dot{\hat{x}}_1(t) = x_2(t) + c_1\,(y(t) - \hat{x}_1(t)) \tag{11}$$

$$\dot{\hat{x}}_2(t) = x_3(t) + b_0\cdot u(t) + c_2\,(y(t) - \hat{x}_1(t)) \tag{12}$$

$$\dot{\hat{x}}_3(t) = c_3\,(y(t) - \hat{x}_1(t)) \tag{13}$$

where c_1, c_2, and c_3 are parameters of the ESO that ensure the estimation of $y, \dot{y}$, and f through the corresponding $\hat{x}_1, \hat{x}_2$, and $\hat{x}_3$. In that case, the control law can be chosen as:

$$u(t) = \frac{K_P(r(t) - \hat{y}(t)) - K_D\dot{\hat{y}}(t) - \hat{f}(t)}{b_0} \tag{14}$$

where $r(t)$ is the setpoint, K_P and K_D are the parameters of the controller.

As a main point of ADRC, an Extended State Observer (ESO) is constructed to estimate the value of f, thereby compensating for the effect of f on the model. Subsequently, the differential equation of the system (Eq. (10)) will be transformed into:

$$\ddot{y}(t) \approx K_P(r(t) - \hat{y}(t)) - K_D\dot{\hat{y}}(t) \tag{15}$$

Applying the Laplace transform to the Eq. (15), we obtain the transfer function for the closed-loop system as follows:

$$G_{CL}(s) = \frac{Y(s)}{R(s)} = \frac{K_P}{s^2 + K_Ds + K_P} \tag{16}$$

As proposed in Herbst [30] and Chien et al. [31], the parameters of ADRC can be obtained as follows:

- Choose the desired 2% settling time T_{settle}
- K_P and K_D are chosen to get a negative-real double pole,

$$K_P = {s_{CL}}^2, K_D = -2s_{CL} \tag{17}$$

with $s_{CL} \approx -\frac{5.85}{T_{\text{settle}}}$ is closed loop double pole.

- The observer poles must be placed left of the closed-loop such that the observer dynamics must be fast enough, for example:

$$s_{ESO1,2,3} = s_{ESO} \approx k_{ESO}.s_{CL} = (3\ldots10)s_{CL} \tag{18}$$

Then, the observer parameters can be calculated as:

$$c_1 = -3s_{ESO}, c_2 = 3{s_{ESO}}^2, c_3 = -{s_{ESO}}^3 \tag{19}$$

3.2. ETM Input Shaper Concept

Input Shaping, initially proposed by Singer and Seering [32], is a feed-forward technique utilized in control systems to mitigate the effects of unwanted oscillations and vibrations induced by input commands. Consider the second-order transfer function of the vibratory system as:

$$\frac{X(s)}{F(s)} = \frac{\omega_n^2}{s^2 + 2\xi\omega_n s + \omega_n^2} \tag{20}$$

where ω_n is the undamped natural frequency and ξ is the damping ratio. If an input impulse with magnitude A_i is applied to the system at time t_i, then the output response $y(t)$ is determined:

$$y(t) = \sum_{i=1}^{n} \frac{A_i \omega_n}{\sqrt{1-\xi^2}} e^{-\xi\omega_n(t-t_i)} \sin\left(\omega_d\left(t-t_i\right)\right) \tag{21}$$

where $\omega_d = \omega_n\sqrt{1-\xi^2}$

The principle idea of input-shaping control is that an input impulse applied to the vibratory system will cause a residual vibration, then a second impulse with appropriate magnitude A_2 can be applied to the system at an appropriate moment t_2 to suppress this vibration.

Another approach to explain and extend the input shaping technique is an impulse vector [33]. The impulse vector approach presents the impulse response of a vibratory system using a vector. The response (21) of the vibratory system can be presented as a vector in a 2D polar coordinate system with a magnitude I_i and angle θ_i, with

$$I_i = A_i e^{\xi\omega_n t_i}, \theta_i = \omega_d t_i \tag{22}$$

In a positive impulse $(A_i > 0)$, the initial point of the impulse vector is located at the origin of the polar coordinate system. In contrast, the terminal point is located at the origin in a negative impulse $(A_i > 0)$. The impulse vector concept is used to design a new class of input shapers called ETM shapers. In the ETM shaper, the angle between two consecutive vectors is the same, and the magnitude of impulse vectors, except for the first and the last vectors, is the same. In other words, the ETMn shaper (ETM with n impulse vectors) satisfies the following conditions:

$$\theta_1 = 0, \theta_2 = \frac{2\pi}{n-1}, \ldots, \theta_{n-1} = \frac{(n-2)\cdot 2\pi}{n-1}, \theta_n = 2\pi \tag{23}$$

$$I_2 = I_3 = \ldots = I_{n-1} = I_1 + I_n, I_n = mI_1(m > 0) \tag{24}$$

The advantage of this ETMn method is that no matter how many impulse vectors are present, these vectors all fit inside a 2π circle time, equivalent to the ZVD method's shaping time. This paper uses the ETM4 shaper, which includes four impulse vectors as in Fig. 3, is applied.

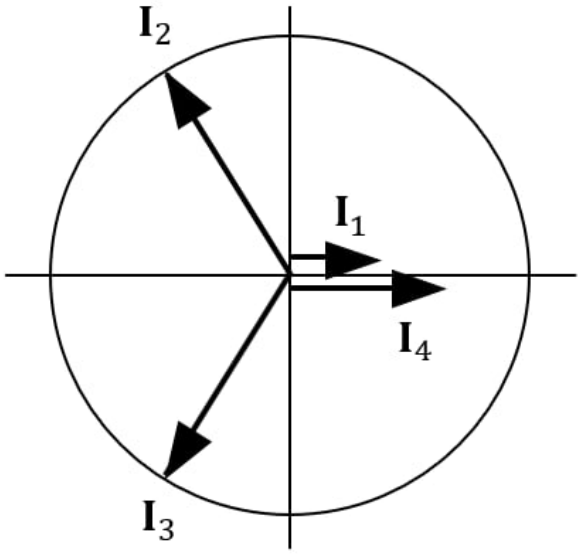

Fig. 3. Impulse vector of ETM4 shaper

The ETM4 shaper impulse instants t_1, t_2, t_3, t_4 are determined by the angles of the impulse vectors. The ETM4 shaper impulse magnitudes A_1, A_2, A_3, A_4 are calculated by solving the following equations:

$$I_1 = A_1 e^{\xi\omega_n t_1}, t_1 = 0 \tag{25}$$

$$I_2 = A_2 e^{\xi\omega_n t_2}, t_2 = \frac{2\pi}{3\omega_d} \tag{26}$$

$$I_3 = A_3 e^{\xi\omega_n t_3}, t_3 = \frac{4\pi}{3\omega_d} \tag{27}$$

$$I_4 = A_4 e^{\xi\omega_n t_4}, t_4 = \frac{2\pi}{\omega_d} \tag{28}$$

$$I_2 = I_3 = I_1 + I_4, I_4 = mI_1(m > 0) \tag{29}$$

$$A_1 + A_2 + A_3 + A_4 = 1 \tag{30}$$

The ETM4 shaper is:

$$\begin{bmatrix} t_i \\ A_i \end{bmatrix} = \begin{bmatrix} 0 & \frac{2\pi}{3\omega_d} & \frac{4\pi}{3\omega_d} & \frac{2\pi}{\omega_d} \\ \frac{I}{1+m} & \frac{I}{K^{\frac{2}{3}}} & \frac{I}{K^{\frac{4}{3}}} & \frac{mI}{(1+m)K^2} \end{bmatrix} \tag{31}$$

where

$$I = \frac{(1+m)K^2}{K^2 + (1+m)\left(K^{\frac{2}{3}} + K^{\frac{4}{3}} + m\right)} \tag{32}$$

$$K = e^{\frac{\xi\pi}{\sqrt{1-\xi^2}}} \tag{33}$$

To determine the optimal value of m, a performance index J is defined as the integral along the sensitivity curve with a sensitivity ratio in a considered range, for example, 0.2 to 1.8 .

$$J = \int_{r_u}^{r_l} V(r,m)dr, r = \frac{\omega_n}{\hat{\omega}_n}, m = \frac{I_n}{I_1}, r_l = 0.2, r_u = 0.8 \tag{34}$$

The optimal values m_{otp} for various ETMn shapers are presented in Kang [33] where $m_{otp} = 1$ if damping ratio $\xi = 0$.

3.3. Modified ETM Shaper in case of payload hoisting

During the payload hoisting process, the cable length l_1 will be changed, which will cause time-varying vibration frequencies. ETM4 Shaper is applied with the calculated frequencies chosen using two averaging schemes to solve the time-varying frequencies. The first scheme uses the average of all operated frequencies, yielding the Average Operating Frequency-ETM4 (AOF-ETM4). The second scheme uses the frequency corresponding to the average of all operated cable lengths, called the Average Operating cable Length-ETM4 (AOL-ETM4). The ETM shaper, in principle, can only suppress the vibration with constant frequency. However, the robustness of ETM can allow vibration suppression with time-varying frequencies.

4. Simulation result

Simulation is conducted to verify the effectiveness of the proposed control scheme. The system parameters for simulation are set according to the 2D experimental overhead crane as: $m = 5$ kg, $m_1 = 2$ kg, $m_2 = 0.5$ kg, $D_t = 25$Ns/m, $D_l = 55$Ns/m, $D_1 = D_2 = 0.1$Ns/rad, $l_1 = 0.3 - 1.0m$, $l_2 = 0.1m$. The first simulation scenario is as follows. The trolley is moved from 0 to 1 m by setting the step reference input for the trolley control. At the same time, the payload is lifted by shortening the rope length from 1 m to 0.3 m .

The ADRC parameters for trolley position and cable length controllers are chosen as:

- $b_{0x} = \frac{1}{m+m_1+m_2}; b_{0l} = \frac{1}{m_1+m_2}$,
- $T_{\text{settle}} = 3$ s for both trolley position and cable length controller,
- $s_{ESO} = 100 s_{CL}$ for both trolley position and cable length controller.

Three factors are considered in evaluating the effectiveness of the proposed solution in vibration suppression: the integral absolute error (IAE) value and maximum sway angle of hook (MA1) and load (MA2). The integral absolute error IAE is defined as follows:

$$\text{IAE} = \int_0^\infty \left(|e_1(t)| + |e_2(t)|\right) dt \tag{35}$$

where $e_1(t)$ and $e_1(t)$ are the hook and payload swing angle error with the desired value of 0 degrees. A smaller value of the considered factor indicates the input shaping technique's more effective vibration suppression capability.

We compare the performance of unshaped ADRC, ADRC with AOF-ETM4, and ADRC with AOL-ETM4 while controlling the trolley position and lifting the load simultaneously.

Since the exact values of the damping ratios are difficult to determine in reality and small, the damping ratio for the computed parameters of these shapers will be chosen as 0 .

For the AOF-ETM4 method, the parameters of two shapers are respectively:

$$\begin{bmatrix} t_i \\ A_i \end{bmatrix} = \begin{bmatrix} 0 & 0.4916 & 0.9834 & 1.4751 \\ 0.1667 & 0.3333 & 0.3333 & 0.1667 \end{bmatrix}$$
$$\begin{bmatrix} t_i \\ A_i \end{bmatrix} = \begin{bmatrix} 0 & 0.1759 & 0.3518 & 0.5277 \\ 0.1667 & 0.3333 & 0.3333 & 0.1667 \end{bmatrix}$$

For the AOL-ETM4 method, the parameters of two shapers are respectively:

$$\begin{bmatrix} t_i \\ A_i \end{bmatrix} = \begin{bmatrix} 0 & 0.5507 & 1.1015 & 1.6523 \\ 0.1667 & 0.3333 & 0.3333 & 0.1667 \end{bmatrix}$$
$$\begin{bmatrix} t_i \\ A_i \end{bmatrix} = \begin{bmatrix} 0 & 0.1780 & 0.3559 & 0.5338 \\ 0.1667 & 0.3333 & 0.3333 & 0.1667 \end{bmatrix}$$

From Fig. 4a, all the control schemes, including unshaped ADRC, ADRC with AOFETM4 and ADRC with AOL-ETM4, effectively control the position of the trolley, following the desired set point with a relatively small overshoot, less than 0.1%. Furthermore, it also shows that the ADRC controller demonstrates effective disturbance cancellation, especially in the case of large load fluctuation angles. Incorporating proposed shapers slightly slow down the position response of the trolley. The ADRC model with AOL-ETM4 has a response time of approximately 4.2611 seconds, approximately the same as the AOF-ETM4 models, with processing times of 4.1319 seconds, respectively.

Regarding cable length in Figure 4b, the response times of the models are relatively similar. Furthermore, the overshoot in all plots is relatively small, the highest being only about 0.985%. Like position feedback control, all cable length control models demonstrate effective disturbance cancellation caused by load fluctuations.

In Figs. 4c and 4d, the unshaped ADRC controller has the fastest response time, so the two shaking angles will have the strongest fluctuations. The IAE, MA-hook and MAload values are 168.7248 degree, 24.4704 degree and 22.7625 degree, respectively (Table 1). However, by incorporating ETM4 shapers, the ability to suppress vibrations is significantly improved. Among the proposed approaches, AOL-ETM4 showed the most effective vibration suppression, reducing IAE, MA-hook and MA-load by 85.62%, 80.05% and 82.26% compared to the unshaped ADRC controller.

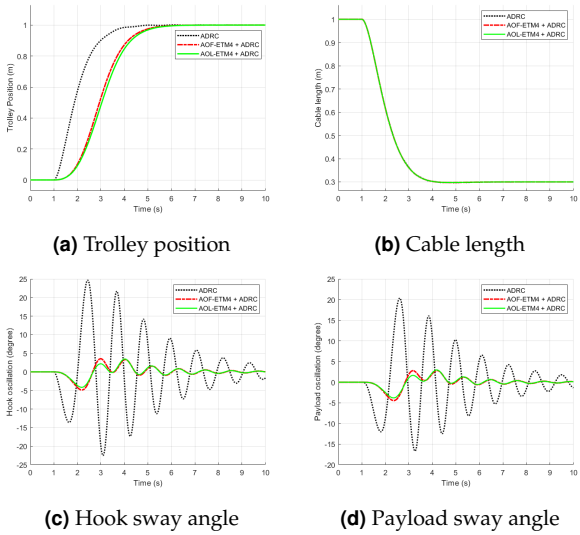

(a) Trolley position **(b)** Cable length

(c) Hook sway angle **(d)** Payload sway angle

Fig. 4. First simulation scenario results

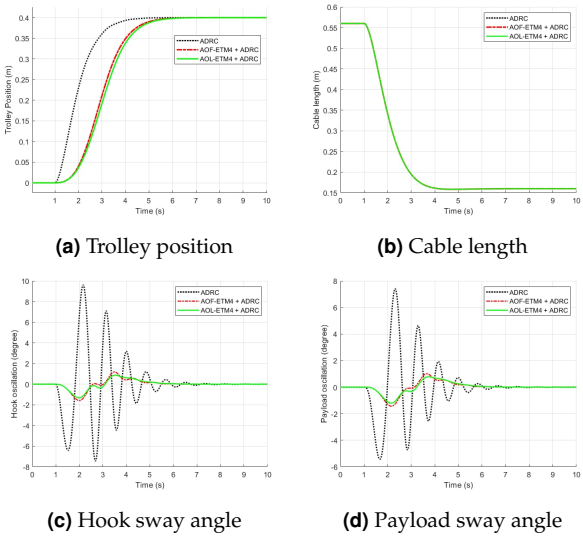

(a) Trolley position **(b)** Cable length

(c) Hook sway angle **(d)** Payload sway angle

Fig. 5. Second simulation scenario results

Table 1. Sway Angle first in simulation

Control scheme	IAE	MA_1	MA_2
Unshaped ADRC	168.7248	24.4704	22.7625
AOL-ETM4+ADRC	24.2672	4.1736	4.0365
AOF-ETM4+ADRC	27.8034	4.8807	4.7318

The second simulation scenario is also considered. In this scenario, the simulation setup is changed, but the controller parameters are kept as in the first scenario. The trolley is moved from 0 to 0.4 m . At the same time, the payload is lifted by shortening the rope length from 0.56 m to 0.16 m, $l_2 = 0.2$ m, $m_1 = 0.5$ kg, $m_2 = 0.5$ kg. The results in Fig. 5 also represent the good performance of the proposed method in trolley position control and vibration control.The IAE, MA-hook and MA-load values are respectively shown in Table 2).

Table 2. Sway Angle in second simulation

Control scheme	IAE	MA_1	MA_2
Unshaped ADRC	41.7670	9.6158	7.4136
AOL-ETM4+ADRC	7.0410	1.3164	1.2062
AOF-ETM4+ADRC	7.6536	1.5814	1.4353

5. Experimental result

In this section, to verify the performance of the proposed method, experiments are conducted with a 2D experimental overhead crane, as shown in Fig. 6 with the system parameters as $m_1 = 0.5$ kg, $m_2 = 0.5$ kg, $l_1 = 0.16 - 0.56$ m, $l_2 = 0.2$ m. The experiment scenario is as follows.

The trolley is moved from 0 to 0.4 m while the payload is lifted by shortening the rope length from 0.56 m to 0.16 m (the same as the second simulation scenario). The trolley and payload hoisting are moved using motors and motor drivers, allowing for precise speed control, where motor velocity can be managed by adjusting the input voltage. Therefore the transfer function for the trolley position control and cable length control in response to a control voltage input can be respectively considered as Solihin et al. [34]:

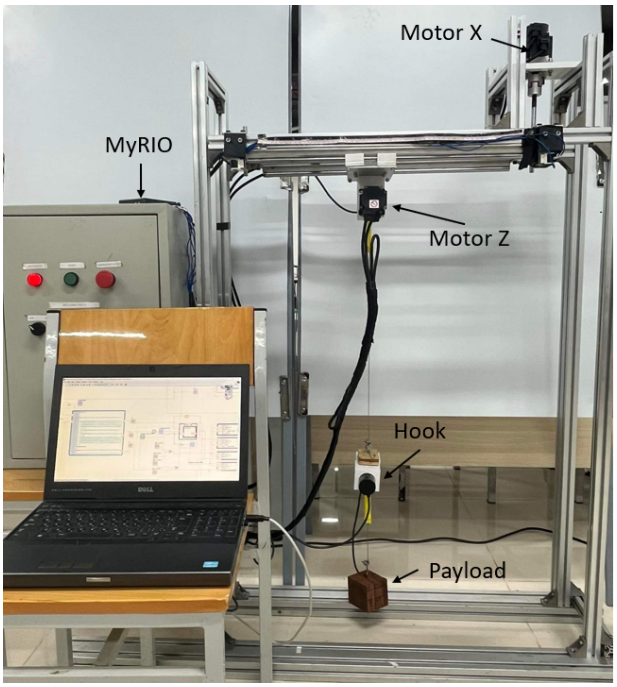

Fig. 6. Experimental model

$$G_x = \frac{X(s)}{U_x(s)} = \frac{K_m}{s\,(T_m s + 1)} \tag{36}$$

$$G_l = \frac{L(s)}{U_l(s)} = \frac{K_l}{s\,(T_l s + 1)} \tag{37}$$

In practice, the amplification coefficients K_m, K_l, and the system time constants T_m, T_l are determined by the model identification process, then, we have the transfer functions between the trolley position and the control voltage, and the cable length and the control voltage are obtained as follows:

$$G_x = \frac{X(s)}{U_x(s)} = \frac{6.1732}{s(0.040898s + 1)} \tag{38}$$

$$G_l = \frac{L(s)}{U_l(s)} = \frac{4.7556}{s(0.040651s + 1)} \tag{39}$$

The parameters for the ADRC controllers in experiments are chosen as:

- $b_{0x} = \frac{6.1732}{0.040898} = 150.94$
  $b_{0l} = \frac{4.7556}{0.040651} = 116.99$
- $T_{\text{settle}} = 3s$ and $s_{ESO} = 100 s_{CL}$ for both trolley position and cable length controller.

For AOF-ETM4 method, the parameters of two shapers are respectively:

$$\begin{bmatrix} t_i \\ A_i \end{bmatrix} = \begin{bmatrix} 0 & 0.3284 & 0.6568 & 0.9852 \\ 0.1667 & 0.3333 & 0.3333 & 0.1667 \end{bmatrix}$$

$$\begin{bmatrix} t_i \\ A_i \end{bmatrix} = \begin{bmatrix} 0 & 0.1642 & 0.3285 & 0.4928 \\ 0.1667 & 0.3333 & 0.3333 & 0.1667 \end{bmatrix}$$

For AOL-ETM4 method, the parameters of two shapers are respectively:

$$\begin{bmatrix} t_i \\ A_i \end{bmatrix} = \begin{bmatrix} 0 & 0.4659 & 0.69318 & 1.3977 \\ 0.1667 & 0.3333 & 0.3333 & 0.1667 \end{bmatrix}$$

$$\begin{bmatrix} t_i \\ A_i \end{bmatrix} = \begin{bmatrix} 0 & 0.1819 & 0.3638 & 0.5458 \\ 0.1667 & 0.3333 & 0.3333 & 0.1667 \end{bmatrix}$$

From Fig. 7a, all the control schemes, including unshaped ADRC, ADRC with AOF-ETM4 and ADRC with AOL-ETM4, effectively control the position of the bridge vehicle, following the desired settling with relatively small overshoot (maximum about 1.94%). Incorporating the ETM4 unit slightly slows down the position response of the bridge vehicle. The ADRC model with AOL-ETM4 has a response time of approximately 3.2250, which is the same as the AOF-ETM4 model, with a processing time of 3.2900 seconds.

From Fig. 7b, it can be seen that all control schemes demonstrated effective control in response to cable length, with relatively similar performance. Although the transient values in all cases are more than 1.2%, these values are still within acceptable limits.

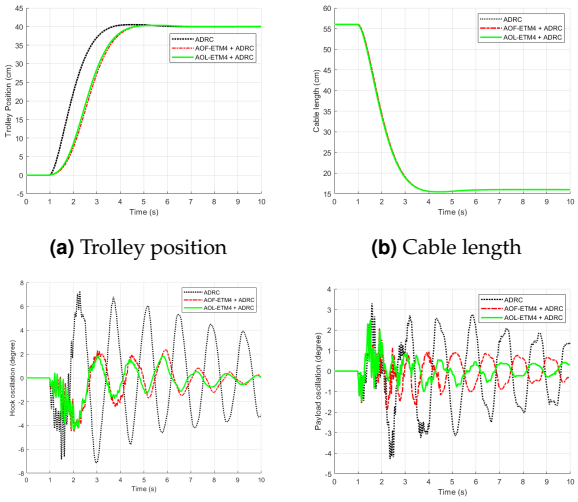

(a) Trolley position **(b)** Cable length

(c) Hook sway angle **(d)** Payload sway angle

Fig. 7. Experiment results

Figs. 7c and 7d demonstrate that incorporating the ETM4 method significantly reduces hook and load-induced oscillations during operation. The effectiveness of the AOL-ETM4 and AOF-ETM4 methods is almost similar. The IAE, MA of hook and load are reduced by 66.40%, 40.11% and 42.11% compared to unshaped ADRC, respectively (Table 3). The proposed controller can reduce the vibration significantly.

Table 3. Sway Angle in experiment

Control scheme	IAE	MA_1	MA_2
Unshaped ADRC	54.6998	7.2882	4.2750
AOL-ETM4+ADRC	18.3771	4.3650	2.4750
AOF-ETM4+ADRC	22.6149	4.5000	2.3850

6. Conclusion

In this study, we propose a method that combines the ETM4 input shaper with an ADRC controller for the double pendulum-type overhead crane system. The ADRC controller can guarantee the precise position tracking of the trolley even with disturbance. The ETM4 input shaper can suppress the multi-mode time-varying frequency vibration of the payload. Two choices of frequency for ETM4 are considered, including the average wire length and average frequency. Simulation and experimental results show that the proposed method helps the system achieve the desired position, significantly reduces residual fluctuations, and ensures the system's stability during operation. Both average wire length and average frequency selection are acceptable for time-varying vibration suppression. In the future, an

adaptive mechanism will be considered to reduce the load vibration with time-variant frequencies further.

References

[1] L. Ramli, Z. Mohamed, A. M. Abdullahi, H. Jaafar, and I. M. Lazim, (2017) *"Control strategies for crane systems: A comprehensive review"* **Mechanical Systems and Signal Processing *95***: 1–23. DOI: https://doi.org/10.1016/j.ymssp.2017.03.015.

[2] H. I. Jaafar, Z. Mohamed, N. A. M. Subha, A. R. Husain, F. S. Ismail, L. Ramli, M. O. Tokhi, and M. A. Shamsudin, (2019) *"Efficient control of a nonlinear double-pendulum overhead crane with sensorless payload motion using an improved PSO-tuned PID controller"* **Journal of Vibration and Control *25***(4): 907–921. DOI: 10.1177/1077546318804319. eprint: https://doi.org/10.1177/1077546318804319.

[3] N. Sun, T. Yang, Y. Fang, Y. Wu, and H. Chen, (2019) *"Transportation Control of Double-Pendulum Cranes With a Nonlinear Quasi-PID Scheme: Design and Experiments"* **IEEE Transactions on Systems, Man, and Cybernetics: Systems *49***(7): 1408–1418.

[4] N. Sun, Y. Wu, Y. Fang, and H. Chen, (2018) *"Nonlinear Antiswing Control for Crane Systems With Double-Pendulum Swing Effects and Uncertain Parameters: Design and Experiments"* **IEEE Transactions on Automation Science and Engineering *15***(3): 1413–1422. DOI: 10.1109/TASE.2017.2723539.

[5] B. Lu, Y. Fang, and N. Sun, (2019) *"Enhanced-coupling adaptive control for double-pendulum overhead cranes with payload hoisting and lowering"* **Automatica *101***: 241–251. DOI: https://doi.org/10.1016/j.automatica.2018.12.009.

[6] L. Yang and H. Ouyang, (2022) *"Precision-positioning adaptive controller for swing elimination in three-dimensional overhead cranes with distributed mass beams"* **ISA Transaction *127***: 449–460. DOI: 10.1016/j.isatra.2021.08.035.

[7] Q. Wu, X. Wang, L. Hua, and M. Xia, (2020) *"Dynamic analysis and time optimal anti-swing control of double pendulum bridge crane with distributed mass beams"* **Mechanical Systems and Signal Processing**: DOI: https://doi.org/10.1016/j.ymssp.2020.106968.

[8] Q. Wu, X. Wang, L. Hua, and M. Xia, (2021) *"Improved time optimal anti-swing control system based on low-pass filter for double pendulum crane system with distributed mass beam"* **Mechanical Systems and Signal Processing *151***: 107444. DOI: https://doi.org/10.1016/j.ymssp.2020.107444.

[9] M. Zhang, Y. Zhang, and X. A. Cheng, (2019) *"Enhanced Coupling PD with Sliding Mode Control Method for Underactuated Double-pendulum Overhead Crane Systems"* **Int. J. Control Autom. Syst *17***: 1579–1488. DOI: 10.1007\s12555-018-0646-0.

[10] H. Ouyang, J. Hu, G. Zhang, L. Mei, and X. Deng, (2019) *"Sliding-Mode-Based Trajectory Tracking and Load Sway Suppression Control for Double-Pendulum Overhead Cranes"* **IEEE Access *7***: 4371–4379. DOI: 10.1109/ACCESS.2018.2888563.

[11] T. Wang, N. Tan, X. Zhang, G. Li, S. Su, J. Zhou, J. Qiu, Z. Wu, Y. Zhai, R. Donida Labati, V. Piuri, and F. Scotti, (2021) *"A Time-Varying Sliding Mode Control Method for Distributed-Mass Double Pendulum Bridge Crane With Variable Parameters"* **IEEE Access *9***: 75981–75992. DOI: 10.1109/ACCESS.2021.3079303.

[12] Q. Wu, X. Wang, L. Hua, and M. Xia, (2021) *"Modeling and nonlinear sliding mode controls of double pendulum cranes considering distributed mass beams, varying roped length and external disturbances"* **Mechanical Systems and Signal Processing *158***: 107756. DOI: https://doi.org/10.1016/j.ymssp.2021.107756.

[13] D. Qian, S. Tong, and S. Lee, (2016) *"Fuzzy-logic-based control of payloads subjected to double-pendulum motion in overhead cranes"* **Automation in Construction *65***: 133–143. DOI: doi.org/10.1016/j.autcon.2015.12.014.

[14] Z. Sun and H. Ouyang, (2022) *"Adaptive fuzzy tracking control for vibration suppression of tower crane with distributed payload mass"* **Automation in Construction *142***: 104521. DOI: https://doi.org/10.1016/j.autcon.2022.104521.

[15] Q. Wu, N. Sun, T. Yang, and Y. Fang, (2024) *"Deep Reinforcement Learning-Based Control for Asynchronous Motor-Actuated Triple Pendulum Crane Systems With Distributed Mass Payloads"* **IEEE Transactions on Industrial Electronics *71***(2): 1853–1862. DOI: 10.1109/TIE.2023.3262891.

[16] M. Kenison and W. Singhose. "Input shaper design for double-pendulum planar gantry cranes". In: *Proceedings of the 1999 IEEE International Conference on Control Applications (Cat. No.99CH36328)*. ***1***. 1999, 539–544 vol. 1. DOI: 10.1109/CCA.1999.806702.

[17] W. E. Singhose, J. Lawrence, K. L. Sorensen, and K. Dooroo, (2006) *"Applications and educational uses of crane oscillation control"* **FME Transactions *34***: 175–183.

[18] K. Chen Chih Peng, W. Singhose, and S. S. Gürleyük. "Initial investigations of hand-motion crane control with double-pendulum payloads". In: *2012 American Control Conference (ACC)*. 2012, 6270–6275. DOI: 10.1109/ACC.2012.6315260.

[19] K. A. Alhazza and Z. N. Masoud, (2016) *"Waveform command shaping control of multimode systems"* **Journal of Sound and Vibration *363***: 126–140. DOI: https://doi.org/10.1016/j.jsv.2015.11.010.

[20] Z. N. Masoud and K. A. Alhazza, (2017) *"A smooth multimode waveform command shaping control with selectable command length"* **Journal of Sound and Vibration *397***: 1–16. DOI: https://doi.org/10.1016/j.jsv.2017.02.049.

[21] S. F. ur Rehman, Z. Mohamed, A. Husain, L. Ramli, M. Abbasi, W. Anjum, and M. Shaheed, (2023) *"Adaptive input shaper for payload swing control of a 5-DOF tower crane with parameter uncertainties and obstacle avoidance"* **Automation in Construction *154***: 104963. DOI: https://doi.org/10.1016/j.autcon.2023.104963.

[22] X. Xie, J. Huang, and Z. Liang, (2013) *"Vibration reduction for flexible systems by command smoothing"* **Mechanical Systems and Signal Processing *39***(1): 461–470. DOI: https://doi.org/10.1016/j.ymssp.2013.02.021.

[23] R. Tang and J. Huang, (2016) *"Control of bridge cranes with distributed-mass payloads under windy conditions"* **Mechanical Systems and Signal Processing *72-73***: 409–419. DOI: https://doi.org/10.1016/j.ymssp.2015.11.002.

[24] Y. Jiahui and H. Jie, (2023) *"Control of Beam-Pendulum Dynamics in a Tower Crane With a Slender Jib Transporting a Distributed-Mass Load"* **IEEE Transactions on Industrial Electronics *70***(1): 888–897. DOI: 10.1109/TIE.2022.3148741.

[25] X. Miao, L. Yang, and H. Ouyang, (2023) *"Artificial-neural-network-based optimal Smoother design for oscillation suppression control of underactuated overhead cranes with distributed mass beams"* **Mechanical Systems and Signal Processing *200***: 110497. DOI: https://doi.org/10.1016/j.ymssp.2023.110497.

[26] D. Minh Duc, N. Van Minh, D. Quy Thinh, and D. Trong Hieu, (2023) *"Reference response based time-varying vibration suppression control for flexible dynamic systems"* **Journal of Engineering Science and Technology *18***(1): 604–623.

[27] D. Gruyter. *Anti-sway Control for Cranes: Design and Implementation Using MATLAB*. De Gruyter, 2017.

[28] W. Singhose, D. Kim, and M. Kenison, (2008) *"Input Shaping Control of Double-Pendulum Bridge Crane Oscillations"* **J. Dyn. Sys., Meas., Control *130***(3): DOI: doi:10.1115/1.2907363.

[29] J. Han, (2009) *"From PID to Active Disturbance Rejection Control"* **IEEE Transactions on Industrial Electronics *56***(3): 900–906. DOI: 10.1109/TIE.2008.2011621.

[30] G. Herbst, (2013) *"A Simulative Study on Active Disturbance Rejection Control (ADRC) as a Control Tool for Practitioners"* **Electronics 2**(3): 246–279. DOI: 10.3390/electronics2030246.

[31] T. M. Chien, D. T. Hieu, and D. Q. Thinh, (2022) *"Development of a Rehabilitation Robot: Modeling and Trajectory Tracking Control"* **ASEAN Engineering Journal *12***(4): 121–129. DOI: 10.11113/aej.v12.17196.

[32] N. C. Singer and W. P. Seering, (1990) *"Preshaping command inputs to reduce system vibration"*:

[33] C. G. Kang, (2019) *"Impulse Vectors for Input-Shaping Control: A Mathematical Tool to Design and Analyze Input Shapers"* **IEEE Control Systems Magazine *39***(4): 40–55. DOI: 10.1109/MCS.2019.2913610.

[34] M. I. Solihin, Wahyudi, and A. Legowo, (2010) *"Fuzzy-tuned PID Anti-swing Control of Automatic Gantry Crane"* **Journal of Vibration and Control *16***(1): 127–145. DOI: 10.1177/1077546309103421. eprint: https://doi.org/10.1177/1077546309103421.